Aerodynamics of Nasal Airways with Application to Obstruction

F. CHOMETON*, P. GILLIERON*, J. LAURENT*
D. EBBO**, P. KOïFMAN***, F. LECOMTE**, N. SORREL-DEJERINE**

* Laboratoire d'Aérodynamique EA1408, CNAM, 15 rue Marat 78210 St Cyr l'Ecole, France
** Hôpital St Michel, Service ORL, 15 rue Olivier de Serres, 75015 Paris, France
*** Hôpital St Michel, Service Radiologie 15 rue Olivier de Serres, 75015 Paris, France

ABSTRACT The Ear, Nose, and Throat and Radiology departments of the Saint Michel Hospital of Paris, and the Aerodynamic Laboratory (EA1408) of the Conservatoire National des Arts et Métiers have been cooperating on a research program to study air flow in the human nasal cavity. The nasal airway resistance measured with flow pressure curves through active anterior rhinomanometry shows that the flow is either laminar or transitional for pathologically choked nasal cavities. After a vasoconstrictor or a surgical operation, the flow becomes turbulent with a constant loss coefficient. The numerical simulation presented deals with a normal nasal airway. The velocity, vorticity and pressure fields, and the pathlines, enable us to identify the functions of the nasal cavity structural components. The fully turbulent aspect of the flow is confirmed by a numerical rhinomanometry flow pressure curve.

Key words: Nasal airways, Obstruction, Rhinomanometry, Numerical simulation.

1. INTRODUCTION

The Ear, Nose and Throat and Radiology departments of the St Michel Hospital of Paris and the Aerodynamic laboratory (EA1408) of the Conservatoire National des Arts et Métiers, have been cooperating on a research program on the aerodynamics of the nasal airways. The aim of this collaborative project is to quantify the nasal obstruction in order to objectify this symptom and to develop the means to perform functional explorations. The proposed approach is based on the analysis of the clinical results obtained from rhinomanometric curves and on the numerical simulation of the flow patterns in the nasal airways.

An anatomic description of the nasal airways, separated by the septum, is shown in Figure 1. By following the air current during the inspiration phase in the left nasal cavity, we first find the nostril, with its rounded edges, followed by the nasal valve. This canal widens at the inferior, middle and superior turbinates, which play the role of aerodynamic guides, heat exchangers and humidifiers for the air inhaled. These turbinates define passages for the air, called meatus, the middle meatus, for example, being located under the middle turbinate. The two nasal airways terminate in the nasopharynx. The upper portion of the nasal airways contains the olfactory slits. The inhaled air is filtered by the nasal hairs located in the nostrils and also by the presence of the mucus lining the cavity walls. This 10 µm thick mucus captures the particles and moves backward under the action of the vibris. The nasal cavities also communicate with the cranial cavities, from front to back, the front air-sinuses, the maxillary sinuses, the ethmoidal cells and the sphenoidal sinuses. The nasal airways play a role in breathing, olfaction and phonation. In rest breathing, the airflow for a nasal cavity is about 180 cm^3/s with a nasal pressure drop of about 50 Pa between the nostril and the nasopharynx. The flowrate reaches 600 to 700cm^3/s and the pressure drop about 400 Pa during exercise.

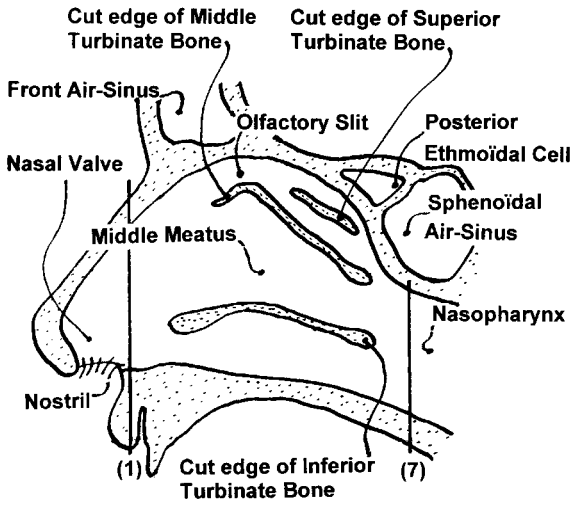

Fig. 1 – Sagittal view of the outer wall of the right nasal airway. The turbinate bones are removed.

Modifications of the geometry of the nasal airways due to a deviation of the septum and/or hypertrophy of the turbinates cause a decrease in the cross-section of the meatus and obstruction of the nasal airways leading to very difficult breathing through the mouth. If the breathing difficulty cannot be eliminated by medication, surgery is considered, very often consisting of a septoplasty and/or turbinectomy of the inferior turbinate. This surgery, which is aimed to restore a normal head loss coefficient for the nasal airways, normally solves the problem. However, the restoration of a normal cross-section for the airflow may be accompanied by a decrease or loss of olfaction or a feeling of abnormal breathing. According to Keyhani *et al*, [1] , the latter could be caused by a lack of information on the wall friction τ_p transmitted by the trigeminal receptors and interpreted as an obstruction, or by poor

aerothermal exchange causing a painful feeling of dryness.

The Reynolds number of the airflow in the nostril, around 2000 in rest breathing, corresponds to a transition flow for a smooth circular duct. A record obtained using a hot wire anemometer positioned 4 mm outside the nostril (see Figure 2) clearly shows the turbulent character of the flow during the exhalation phase, when the velocity is larger than 1.5 m/s. Since the anemometer is located outside the nasal airways, this measurement does not offer positive information on the type of flow for the inhalation phase.

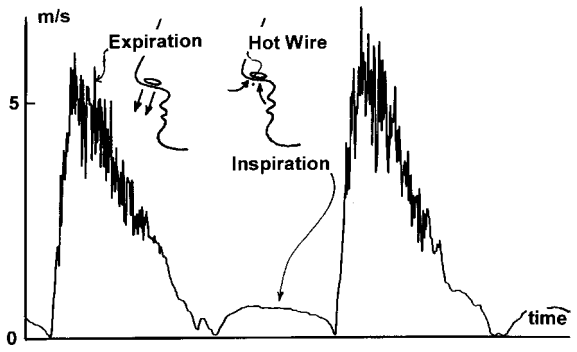

Fig. 2 – Velocity measurement 5 mm outside the nostril during rest breathing

Obstruction problems stem from the aerodynamics and can be analyzed using experimental or numerical models. Elad *et al* , [2] performed calculations on the region lying between the nasal orifice and the nasopharynx. The flow is assumed to be laminar. The numerical simulation, carried out for linearized three-dimensional equations, is made with the FIDAP finite elements code. The results obtained related to a geometry represented by a combination of plane surfaces supplying trapezoidal coronal and sagittal sections. The advantage of these calculations based on a simplified geometry is to allow simulation without the turbinates, and then with the inferior turbinate alone, and finally with both turbinates. The results obtained reveal the role of the olfactory slit and the inferior and middle meatus. The authors also show that the flow structures in inhalation and exhalation are similar. Kimbell *et al*, [3] also use the FIDAP code to calculate the velocities in the nasal airways of the rat for the inhalation and transfer of a toxic gas in the mucus. The geometry is three-dimensional and the flow is laminar based on a Reynolds number of about 300. The calculated velocities, compared with the velocities measured using visualizations by dyes in water are satisfactory. Keyhani *et al*, [1] use the same type of approach for humans for the inhalation and exhalation phases. The geometry is three-dimensional, the FIDAP code is used, and the fluid volume lying between the nostril and a coronal plane located at the level of the choanes is discretized using about 170,000 elements. The numerical results show good agreement with the results obtained on a 1:20 scale model, Hahn *et al*, [4]. Their conclusions on the laminar nature of the flow appear to disagree partially with the experimental results obtained by Girardin *et al*, [5] on a model of human nasal airways constructed from a silicone imprint made on a corpse. Girardin *et al* conclude that the velocity profiles recorded by LDV are typical of a turbulent flow, although the Reynolds number indicates laminar flow. Naftali *et al*, [6] use the same model as Elad *et al*, [2], as well as the FIDAP code, to calculate transport mechanisms in laminar conditions in the nasal airways in the inhalation phase. The role of the turbinates on heat exchanges and on moisture transport is revealed, successively during exercise and for choked nasal airways. The authors also analyze the situation in which the input of the blood flow in the nasal wall, strongly vascularized, is reduced, and also for extreme environmental situations, hot/humid, dry/cold and cold/humid.

The difficulty associated with the laminar or turbulent nature can be removed, for exhalation and inhalation, by making calculations for the upper respiratory tract. This type of approach, which takes account of the nasal airways, the larynx, the trachea and the bronchus, is proposed by Yu *et al.*, [7]. The geometry of the domain is simplified and the calculations are performed basically assuming laminar flow.

This problematics also surrounds the analysis of the deposition of inhaled particles. The aim is to predict the therapeutic or toxic effects of a product. Martonen *et al*, [8] propose a physical model based on an axisymmetrical two-dimensional representation of the upper respiratory tract. Yu *et al*, [9] adopt a model based on the statistical analysis of the aerosol concentrations at the inlet of the nostril, and at the outlet of the mouth, on a subject holding his breath. A complete bibliography of the predictive models associated with this type of problem is given by Hubal *et al*, [10]. The experimental work of Girardin *et al* provides a very complete database.

2. PHYSICAL ANALYSIS

Rhinomanometry – From a clinical standpoint, the airflow in the nasal airways can be analyzed by active anterior rhinomanometry, Eichler, [11]. With the nasal airways shown roughly as in Figure 3, the instrument measures the head loss Δp between point (A) located in the right nostril (for example) and the atmosphere. The velocity is zero in this nasal cavity and the pressure at point (A) is equal to the stagnation pressure at the nasopharynx (point B). Hence the instrument measures the head loss Δp between the nasopharynx and the atmosphere for the left nostril. This measurement accounts for the head loss associated with the opening of the nostril orifice to the atmosphere for inhalation and exhalation. The flowrate Q_v is measured on the left nostril by a diaphragm flowmeter. A reading obtained on at ATMOS 200 rhinomanometer is shown in Figure 4.

The presentation (Q_v, Δp) of the results conforms to the recommendations of the Standardization Committee, Stevens *et al*, [12]. In Figure 4, the "normal" nasal airway corresponds to curve (1). The symmetry of this curve about the origin shows that the head losses are identical for inhalation and exhalation. This suggests that if the flow is transitional or turbulent in the exhalation phase, see Figure 2b, it should also be so in the inhalation phase.

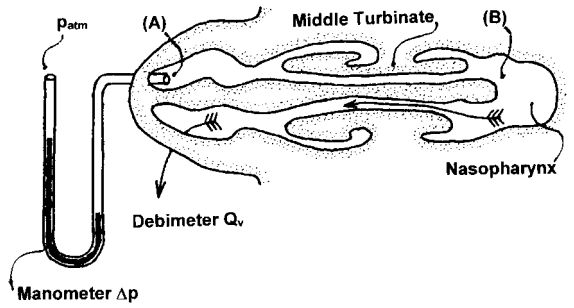

Fig. 3 – Active anterior rhinomanometry. (Axial view)

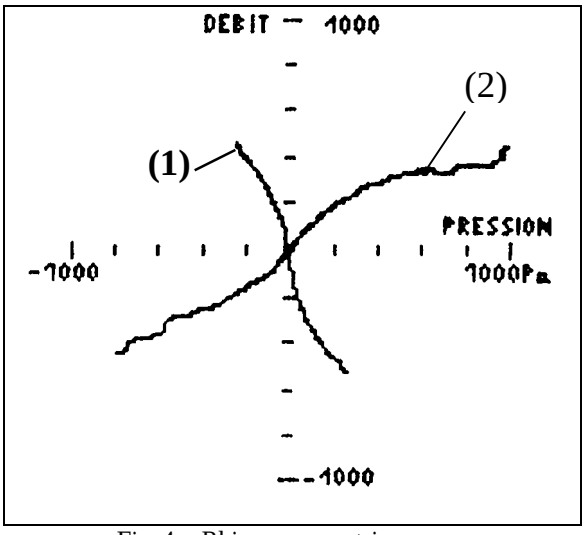

Fig. 4 – Rhinomanometric curves,
(Flowrate (cm^3/s), Head Loss (Pa))

(i) Obstruction is evaluated clinically from the breathing resistance R defined by the ratio $R = \frac{\Delta P}{Q_v}$ which is expressed in $Pa.s/cm^3$ in rhinomanometry. This type of approach is implicitly based on the linear flow pressure law and probably on the assumption of laminar flow.

(ii) The shape of curves (Qv, Δp), shown in Figure 5, suggests quantifying nasal obstruction by the ratio, Eichler, [13], Chometon, *et al* [14], $O = \frac{\Delta P}{Q_v^2}$. This ratio, called the obstruction coefficient here, is expressed in $Pa.s^2/cm^6$. The coefficient O is a function of the head loss coefficient $K = \frac{\Delta P}{\frac{1}{2}\rho U_v^2}$ and a diameter D characteristic of the canal. In turbulent flow, the obstruction coefficient O varies with K, i.e. it decreases as a function of the Reynolds number and generally tends towards a constant in fully turbulent flow.

(iii) A rhinomanometer can also be used to evaluate the pressure P (in Watts) associated with breathing, Eichler, [15] by $P = \Delta p \cdot Q_v$

Analysis of a clinical case - The rhinomanometric curves plotted on a clinical case before and after vasoconstrictor for a right nasal airway in inhalation are shown in Figure 5. The patient displays a wide septum deviation with hypertrophy of the inferior turbinates. The maximum flowrate before vasoconstriction (VC) is 350 cm^3/s at 700 Pascal. It reaches 725 cm^3/s at 500 Pa after vasoconstriction. Post-processing of these clinical curves allows calculation of the resistance R and the obstruction coefficient O, which evolves as a function of the flowrate as shown in Figures 6 and 7.

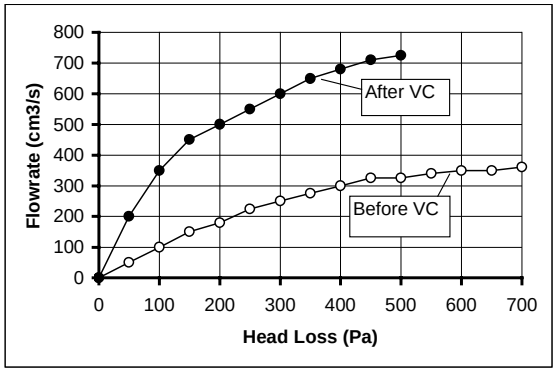

Fig. 5 – Rhinomanometric curves in the inhalation phase, before and after vasoconstriction.

Before VC, the resistance R is constant and equal to 1 for flowrates from 0 to 150 cm^3/s. The choked flow is hence laminar for a low flowrate. Above 150 cm^3/s, the value of R increases, suggesting a tendency towards a transition flow. This is confirmed by the analysis of the obstruction coefficient O, before VC, which decreases as a function of flowrate, see Figure 7.

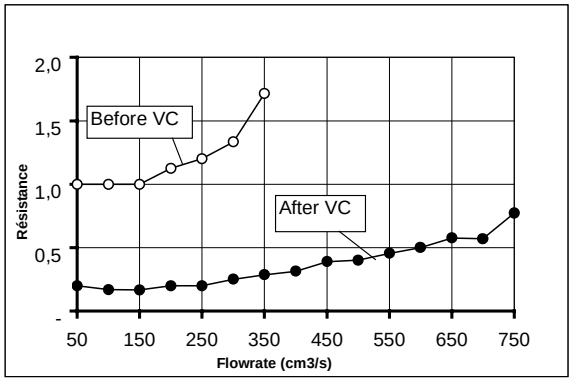

Fig. 6 – Resistance R as a function of flowrate Q_v

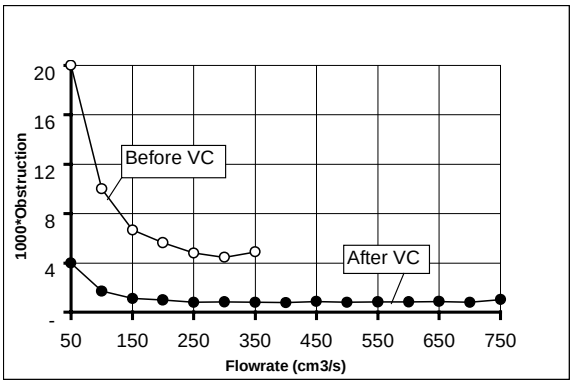

Fig. 7 – Obstruction O as a function of flowrate

After VC, the resistance R of the nasal airway is lower. The value of R, close to 0.20 up to 250 cm^3/s, then increases. This suggests that for flowrates above 250 cm^3/s, the flow becomes turbulent. This is confirmed by the analysis of the obstruction coefficient O, see Figure 7, for the curve obtained after VC. Up to 250 cm^3/s the coefficient O decreases, indicating an influence of the Reynolds number. Above this flowrate, the obstruction O is constant, the flow becoming fully turbulent. The associated power curves show that to reach a breathing rate of 350 cm^3/s, the patient must supply a power six times greater if the nasal airways are obstructed, easily explaining the difficulty felt.

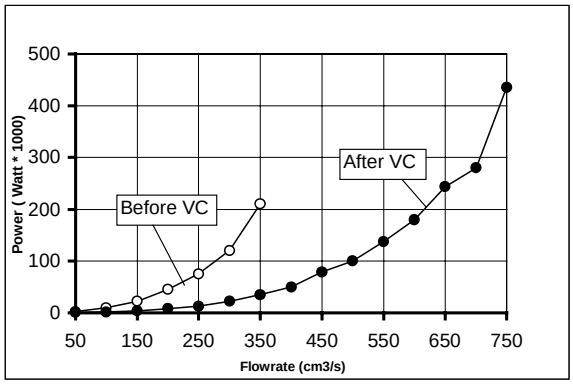

Fig. 8 – Power absorbed by a nasal airway before and after vasoconstriction.

3. NUMERICAL SIMULATION

The numerical results presented concern the calculation of the flow in a right nasal airway from the nostril to the nasopharynx for the inhalation phase. The calculations are three-dimensional and made in turbulent flow with the FLUENT industrial code, of the finite volume type. In the absence of clinical results for this geometry at this stage of the investigations, the results are analyzed and compared with the results from the bibliography, particularly those of Girardin *et al.*

Modeling – The geometry of the calculation domain, defined from the tomodensitometric sections plotted with a 5 mm step in the coronal and axial planes, provide a good definition of the turbinates and the nasal valve. Since these curves are obtained on a patient and hence do not readily provide information on the sections downstream of the choanes, the choanal arc and the nasopharynx have been defined numerically from the most posterior sections. The different sinuses and their connecting channels with the nasal airway are not modeled. The geometry of the volume is visualized by means of several coronal sections shown in Figure 9, Chometon *et al*, [15]. Sections (1) and (6) are located respectively in the nasal valve and 5 mm in front of the nasopharynx, of which the inlet is shown by section (7). The flow is assumed to be turbulent and incompressible. For the inhalation phase, a velocity V_0 normal to the inlet section of the outer nostril is imposed. A pressure condition is imposed at the outlet. The turbulence model is of the k-ε type associated with a log wall law. This boundary condition treats the wall of the nasal airway as a smooth, non-wavy solid wall, and ignores the presence of mucus and its movement. The results presented correspond to a velocity V_0 = 4.17 m/s at the inlet, or a flowrate of 200 cm^3/s. The Reynolds number related to diameter D of the nasal orifice is Re = 2200. The turbulence ratio imposed at the inlet is 1%. The calculations and the post-processing of the results are carried out on a Silicon Graphics Octane type station. The numerical scheme used is of the first order and the solution is converged after about 600 iterations. Calculation time is close to 50 hours. The triangular surface mesh has 102,000 elements. The average distance between two consecutive nodes is 0.5 mm. This distance represents 1/15 of the diameter of the nasal orifice. The volumetric mesh has 500,000 tetrahedral cells.

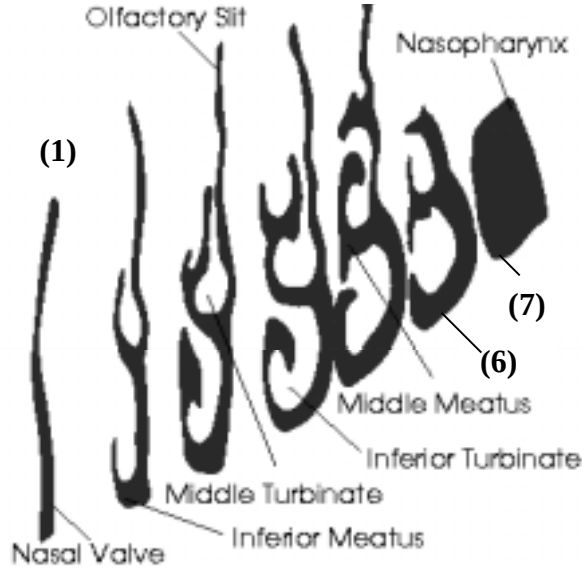

Fig. 9 – Geometry of the right nasal airway. Front view. Coronal sections (1) and (7) are identified in Figure (1)

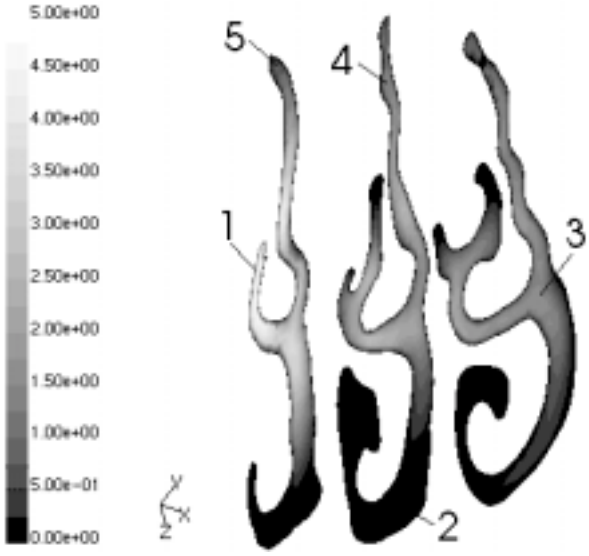

Fig. 10 – Iso-velocity curves, coronal sections

Aerodynamic field – The flowrate distribution in the nasal airway is analyzed from the iso-velocity contours shown in Figure 10. The velocity is a maximum in the middle meatus, point (1), and drops from 4.4 m/s at point (1) to 1.6 m/s at point (3). The velocity is very low in the

inferior meatus and about 0.12 m/s at point (2). The same applies in the olfactory slit where the velocity is 0.62 m/s at point (5) and then rises to 1.37 m/s at point (4). The rotation of the fluid around the inferior turbinate is confirmed by tracking particles uniformly distributed in the nasal orifice. The results show that the fastest particles reach the self-digestive junction at point (A). The particles rotated by the inferior turbinate reach point (B). At the same time, the particles located in the anterior portion of the nasal orifice reach points (C) and (D). These results agree with those of Keyhani *et al* and Girardin *et al.* The calculations show that the static pressure loss occurs in the inferior meatus. The static pressure is virtually uniform in the olfactory slit. The head loss is located in the nasal valve, see Figure 12. The stagnation pressure drops from 35 Pa in the nostril to 29.2 Pa at point (1) and then to 19.3 Pa at point (2). Downstream, the stagnation pressure varies slightly and goes from 9.4 Pa at point (3) to 4.4 Pa at point (4). The pressure is constant in the olfactory zone point (5). Its value of 9.4 Pa at point (5) reaches 6.1 Pa at point (6). The analysis of the rotational field shows that the vortices are located at the walls, in the boundary layers. This result suggests that the flow is rotated by the turbinates without the production of vorticity and hence without any associated pronounced head loss.

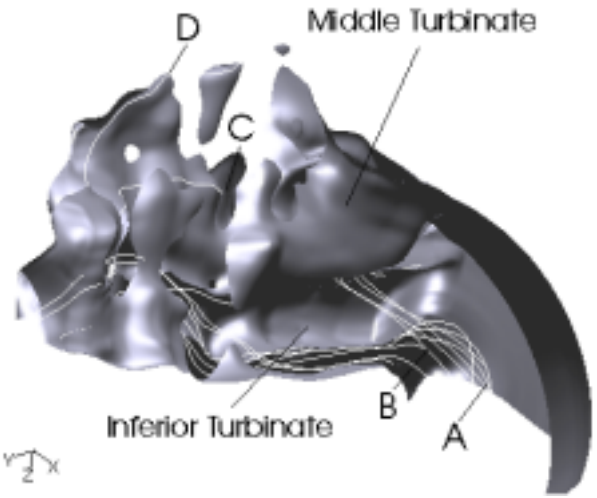

Fig. 11 – Particle trajectories, sagittal section

Fig. 12 – Total pressure, coronal sections.

Numerical rhinomanometric curve – The calculations are supplemented by the determination of a numerical rhinomanometric curve obtained by varying the flowrate from 0 to 1000 cm^3/s, see Figure 13. The curve is qualitatively similar to the measured curve shown in Figure 5, after VC. The calculation also serves to obtain the resistance R and the obstruction coefficient O, see Figures 14 and 15.

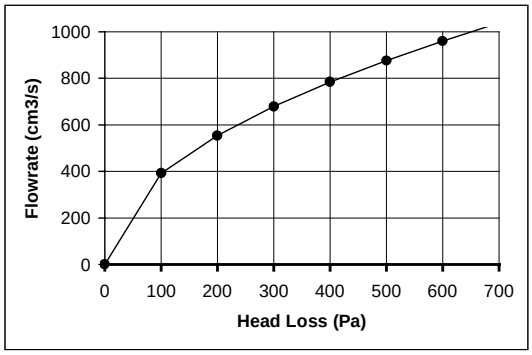

Fig 13 – Numerical rhinomanometric curve

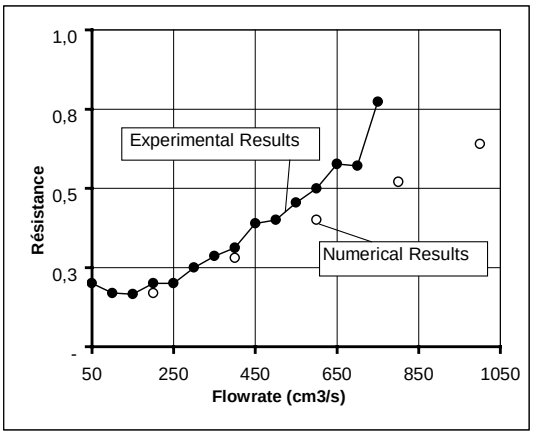

Fig 14 – Numerical resistance coefficient R as a function of flowrate (the continuous curve is shown for reference, see Figure 6).

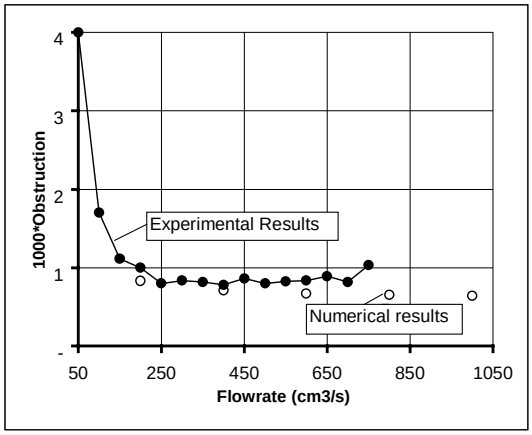

Fig 15 – Numerical obstruction coefficient O as a function of flowrate (the continuous curve is shown for reference, see Figure 7)

The curves of the resistance and obstruction coefficients in Figures 6 and 7 are shown in Figures 14 and 15 for qualitative comparison. The calculation

shows that the obstruction coefficient O obtained for healthy nasal airways increases slightly as a function of flowrate. This suggests that the present calculation does not account for the fully turbulent nature of the flow measured for the healthy or treated nasal airways, see Figure 6.

4. CONCLUSIONS

The detailed knowledge of the aerodynamic behavior of the nasal airways provides aid for decisions in the surgical treatment of nasal obstruction, and also a means of ex post facto analysis. The analysis of the clinical rhinomanometric curves shows that the obstruction coefficient O, used in addition to the standardized resistance coefficient R, serves to confirm the turbulent nature of the flow in the healthy and treated nasal airways when the breathing rate is above 200 cm^3/s. This results agrees with the proposals of Schumacher *et al*, [16]. The numerical simulation, carried out on healthy nasal airways, shows that the numerical rhinomanometric curves and the resistance and obstruction coefficients can be calculated from the sole knowledge of the geometry of the nasal airways, from the nostril to the nasopharynx. Forthcoming studies address the numerical forecasting of the rhinomanometric curves for a simulated surgery on the septum or the turbinates of obstructed nasal airways. This approach is currently being validated, initially associated with the calculation of the rhinomanometric curves before and after operation on a pathological case. For this type of problem, the effort lies upstream the calculation, where efficient procedures must be developed to obtain sections of nasal airways rapidly via medical imaging and a numerical reconstruction of the volumes from these sections.

Acknowledgements - This work is partially supported by funding from « Fondation Bayer Santé ».

4. REFERENCES

[1] Keyhani K., Sherer P.W., Mozell M.M. – Numerical Simulation of Airflow in the Human Nasal Cavity, Journal of Biomechanical Engineering, Vol. 117, 1995, pp. 429-441.

[2] Elad D., Liebenthal R., Eivan S., Wenig B.L. - Analysis of Air Flow Patterns in the Human Nose, Medical & Biological Engineering & Computing, Nov. 1993, pp. 585-592.

[3] Kimbell J.S., Gross E.A., Joyner D.R., Godo M.N., Morgan K.T. – Application of Computational Fluid Dynamics to Regional Dosimetry of Inhaled Chemicals in the Upper Respiratory Tract of the Rat, Toxicology and Applied Pharmacology, 121, pp 253-263, 1993.

[4] Hahn I., Scherer P.W., Mozell M.M. – Velocity Profiles Measured for Airflow Through a Large-Scale Model of the Human Nasal Cavity, Modelling in Physiology,1993, pp 2273-2287.

[5] Girardin M., Bilgen E., Arbour P. – Experimental Study of Velocity Fields in a Human Nasal Fossa by Laser Anenometry, Ann Otol Rhinol Laryngol, 92, 1983, pp 231-236.

[6] Naftali S., Schroter R.C., Shiner R.J., Elad D. – Transport Phenomena in the Human Nasal Cavity : A computational Model, Annals of Biomedical Engineering, Vol. 26, 1998, pp. 831-839.

[7] Yu G., Zhang Z., Lessman R. – Fluid Flow and Particle Diffusion in the Human Upper Respiratory System, Aerosol Science ans Technology, 28, pp 146-158, 1998.

[8] Martonen T.B., Zhang Z., Lessman R.C. – Fluid Dynamics of the Human Larynx and Upper Tracheobronchial Airways, Aerosol Science and Technology, 19, 1993, pp 133-156.

[9] Yu G., Zhang Z., Lessman R. – Computer Simulation of the Flow Field and Particle Deposition by Diffusion in 3D Human Airway Bifurcation, Aerosol Science and Technology, 25, 1996, pp 338-352.

[10] Cohen Hubal E.A., Fedkiw P.S., Kimbell J.S. – Mass-Transport Models to Predict Toxicity of Inhaled Gases in the Upper Respiratory Tract, Modelling in Physiology, 1996, pp. 1415-1427.

[11] Eichler J. - Theorie zu einigen systematischen MeSfehlern bei der Rhino-Manometrie, (*The Theory of some Systematic Errors of Measurement in Rhinomanometry*), Biomedizinishe Technik, Band 23, 1978, pp.280-284.

[12] Stevens J.C., Jones A.S., Lancer J., Beckingham E. – A Microcomputer-based Procedure for Carrying out Rhinomanometry, Journal of Medical Engineering & Technology, Vol. 11, Number 6 , 1987, pp. 278-281.

[13] Eichler J. – Leistungskurven in der Rhinomanometrie (*Power-Curves in Rhinomanometry*), Biomedizinishe Technik, Band 3, pp.42-45, 1989.

[14] Chometon F, .Ebbo D. , Koïfman P., Lecomte F., Gilliéron P., Sorrel-Dejerine N. - Analyse Scientifique de l'Aérodynamique des Fosses Nasales. Actes 106ème Congrès Paris (France) d'Oto-Rhino-Laryngologie et de Chirurgie de la Face et du Cou, 1999.

[15] Chometon F, .Ebbo D. , Koïfman P., Lecomte F., Gilliéron P., Sorrel-Dejerine N. - Simulation Numérique de l'Ecoulement de l'Air dans les fosses Nasales. Ann. Otolaryngol. Chir. Cervico. Fac., 1999, to be published 2000.

[16] Schumacher M.J., Gaines J.A., Bescript B. – Computer-aided rhinomanometry : Analysis of inspiratory and expiratory nasal pressure-flow curves in subjects with rhinitis, Computers in Biology and Medicine, Vol.15, N°4, 1985, pp. 187-195.